prevent mitochondrial permeability transition, which results in the uncoupling of electron transport[14]. These data suggest that Bcl-2 proteins may directly or indirectly affect the permeability of these important cytoplasmic organelles and thus regulate cellular homeostasis and apoptosis. □

Received 26 February; accepted 11 April 1996.

1. Korsmeyer, S. J. *Trends Genet.* **11,** 101–105 (1995).
2. Boise, L. H. *et al. Cell* **74,** 597–608 (1993).
3. Yin, X.-M., Oltvai, Z. N. & Korsmeyer, S. J. *Nature* **369,** 321–323 (1994).
4. Chittenden, T. *et al. EMBO J.* **14,** 5589–5596 (1995).
5. Boyd, J. M. *et al. Oncogene* **11,** 1921–1928 (1995).
6. Parker, M. W. & Pattus, F. *Trends biochem. Sci.* **18,** 391–395 (1993).
7. Cheng, E. H.-Y., Levine, B., Boise, L. H., Thompson, C. B. & Hardwick, J. M. *Nature* **379,** 554–557 (1996).
8. Borner, C. *J. Cell Biol.* **126,** 1059–1068 (1994).
9. Hanada, M., Aime-Sempe, C., Sato, T. & Reed, J. C. *J. biol. Chem.* **270,** 11962–11969 (1995).
10. Sedlak, T. W. *et al. Proc. natn. Acad. of Sci. U.S.A.* **92,** 7834–7838 (1995).
11. Yang, E. *et al. Cell* **80,** 285–291 (1995).
12. London, E. *Biochim. biophys. Acta* **1113,** 25–51 (1992).
13. Lam, M. *et al. Proc. natn. Acad. Sci. U.S.A.* **91,** 6569–6573 (1994).
14. Zamzami, *et al. J. exp. Med.* **182,** 367–377 (1995).
15. Carson, M. J. *J. Molec. Graph.* **5,** 103–106 (1987).
16. Fang, W., Rivard, J. J., Mueller, D. L. & Behrens, T. W. *J. Immunol.* **153,** 4388–4398 (1994).
17. Otwinowski, Z. *Proceedings of the CCP4 Study Weekend: Isomorphous Replacement and Anomalous Scattering* (eds Wolf, W., Evans, P. R. & Leslie, A. G. W.) 80–86 (SERC Daresbury Laboratory, Warrington, UK, 1991).
18. *CCP4: A Suite of Programs for Protein Crystallography* (SERC Daresbury Laboratory, Warrington, UK, 1979).
19. Jones, T. A., Zou, J.-Y., Cowan, S. W. & Kjelgaard, M. *Acta crystallogr. A* **47,** 110 (1991).
20. Reed, R. J. *Acta crystallogr. A* **42,** 140–149 (1986).
21. Brünger, A. T. *X-PLOR 3.1* (Yale University, New Haven, CT, 1992).
22. Yamazaki, T., Lee, W., Arrowsmith, S. H., Muhandiram, D. R. & Kay, L. E. *J. Am. chem. Soc.* **116,** 11655–11666 (1994).
23. Clore, G. M. & Gronenborn, A. M. *Meth. Enzym.* **239,** 349–363 (1994).
24. Logan, T. M., Olejniczak, E. T., Xu, R. X. & Fesik, S. W. *FEBS Lett.* **314,** 413–418 (1992).
25. Neri, D., Szperski, T., Otting, G., Senn, H. & Wüthrich, K. *Biochemistry* **28,** 7510–7516 (1989).
26. Vuister, G. W., Kim, S.-J., Wu, C. & Bax, A. *J. Am. chem. Soc.* **116,** 9206–9210 (1994).
27. Kuboniwa, H., Grzesiek, S., Delaglio, F. & Bax, A. *J. Biomolec. NMR* **4,** 871–878 (1994).
28. Kuszewski, J., Nilges, M. & Brünger, A. T. *J. Biomolec. NMR* **2,** 33–56 (1992).
29. Farrow, N. A. *et al. Biochemistry* **33,** 5984–6003 (1994).
30. Choe, S. *et al. Nature* **357,** 216–222 (1992).

ACKNOWLEDGEMENTS. We thank T. Holzman, J. Severin, K. Walter and H. Zhang for help in protein preparation; S. Snyder for analytical ultracentrifugation studies; and S.W.M. thanks C. Abad-Zapatero, C. Park and V. Giranda for discussions.

CORRESPONDENCE and requests for materials should be addressed to either S.W.M. (e-mail: muchmore@servo.pprd.abbott.com) or S.W.F. (e-mail: fesik@steves.abbott.com). Coordinates for the NMR and X-ray structures of Bcl-x_L have been deposited in the Brookhaven Protein Data Bank with accession numbers 1LXL and 1MAZ, respectively.

Structure of mitochondrial creatine kinase

Karin Fritz-Wolf, Thomas Schnyder*†, Theo Wallimann* & Wolfgang Kabsch

Max-Planck-Institut für medizinische Forschung, Abteilung Biophysik, Jahnstrasse 29, D-69028 Heidelberg, Germany
* Institute for Cell Biology, Swiss Federal Institute of Technology, ETH-Hönggerberg, CH-8093 Zürich, Switzerland

Creatine kinase (CK; EC 2.7.3.2), an enzyme important for energy metabolism in cells of high and fluctuating energy requirements, catalyses the reversible transfer of a phosphoryl goup from phosphocreatine to ADP[1–3]. We have solved the structure of the octameric mitochondrial isoform, Mi_b-CK, which is located in the intermembrane compartment and along the cristae membranes. Mi_b-CK consumes ATP produced in the mitochondria for the production of phosphocreatine, which is then exported into the cytosol for fast regeneration of ATP by the cytosolic CK isoforms. The octamer has 422 point-group symmetry, and appears as a cube of side length 93 Å with a channel 20 Å wide extending along the four-fold axis. Positively charged amino acids at the four-fold faces of the octamer possibly interact with negatively charged mitochondrial membranes. Each monomer consists of a small α-helical domain and a large domain containing an eight-stranded antiparallel β-sheet flanked by seven α-helices. The conserved residues of the CK family form a compact cluster that covers the active site between the domains.

We have obtained tetragonal crystals of sarcomeric, chicken cardiac Mi_b-CK, both with and without NaATP, which contain half an octamer in the asymmetric unit. The native structure was solved by isomorphous replacement at 5 Å, and phase extension to 3 Å resolution by using the four-fold redundancy of the electron density (Table 1). The monomer (dimensions $\sim 36 \times 42 \times 69$ Å) consists of a small (residues 1–112) and a large domain (residues 113–380), with the substrate-binding site located in the cleft between the domains (Fig. 1). Sequence alignment of the CK isoenzymes[4,5] reveals six highly conserved regions, which form a compact common core of the enzyme involved in substrate binding and catalysis (Fig. 1*a*, *b*). Outside the common core we have identified regions that are involved in isoform-specific functions of Mi_b-CK, such as the formation of octamers or binding to the mitochondrial membrane. The overall chain fold differs from other kinases, although the sequence motif (L_{282}GTGLRAGV_{290}) matches the consensus sequence (LGXGXX$G_{(A,S)}$V) of the P-loop found as a characteristic feature in the protein-kinase family[6]. In CK it extends into strand β_6, and is located too far from the phosphate moiety of ATP for a direct interaction (Fig. 2*a*, bottom). A remote similarity also exists for strands β_6, β_7 and β_8, which are connected like strands 3, 4 and 5 in the catalytic subunit of cyclic AMP-dependent protein kinase (see Fig. 3 ref. 6).

Data analysis of the ATP : Mi_b-CK co-crystals reveals different electron density for the nucleotide in each monomer. Structural details of the nucleotide and its protein environment, as found in monomer A (and similarly in C and D) of the ATP : Mi_b-CK co-crystals are described in Figs 1*a* and 2*a*, *b*. ATP is bound differently in monomer B (Figs 1*b* and 2*c*), such that the adenine ring comes closer to Trp 223. The different locations, as well as the solvent accessibility of the phosphate moiety and the high-temperature factors for all nucleotides and their surrounding loops, suggest that the nucleotides have not reached their final well-defined places required for the phosphoryl-transfer reaction. We speculate that in response to the binding of a magnesium ion and creatine (not present in the crystals), the nucleotide base would be closer to Trp 223 and the phosphates nearer to Asp 228, Glu 227 and Glu 226 (which are good candidates for coordinating the magnesium ion of ATP, as well as for binding creatine), and the loops 60–66 and 316–326 would move nearer the active site to exclude water during catalysis. Indeed, these loops are very flexible in the crystal, as indicated by solvent exposure of hydrophobic residues (Phe 63 and Ile 64), high-temperature factors, and different conformations assumed in the monomers resulting from crystal contacts. Moreover, Ala 323, which is part of the loop 316–326 (Fig. 1*b*), has previously been identified as a cleavage site for proteases, and was thought to be located in an exposed surface loop involved in the substrate-induced conformational changes essential for catalysis[7].

Although none of the nucleotides found in the structure are at the correct places for catalysis, they must be quite close. The peptide regions Val 232 to Lys 237 and Val 275 to Arg 287 in the neighbourhood of the adenine base (Fig. 2*a*) have been photolabelled with azidoadenine nucleotide analogues[8], and many of the active-site residues implicated by various other methods can be identified in the X-ray structure.

Cys 278 (Cys 283 in cytosolic CKs), which is found near the γ-phosphate of ATP (Fig. 2*a*,*b*, bottom) was shown by affinity labelling with epoxycreatine to be located in or near the creatine-binding site[9]. The distance of 10.3 Å between the S_γ atom of Cys 278 and the P_β atom of ATP is in qualitative agreement with

† Present address: MRC Laboratory of Molcular Biology, Hills Road, Cambridge CB2 2QH, UK.

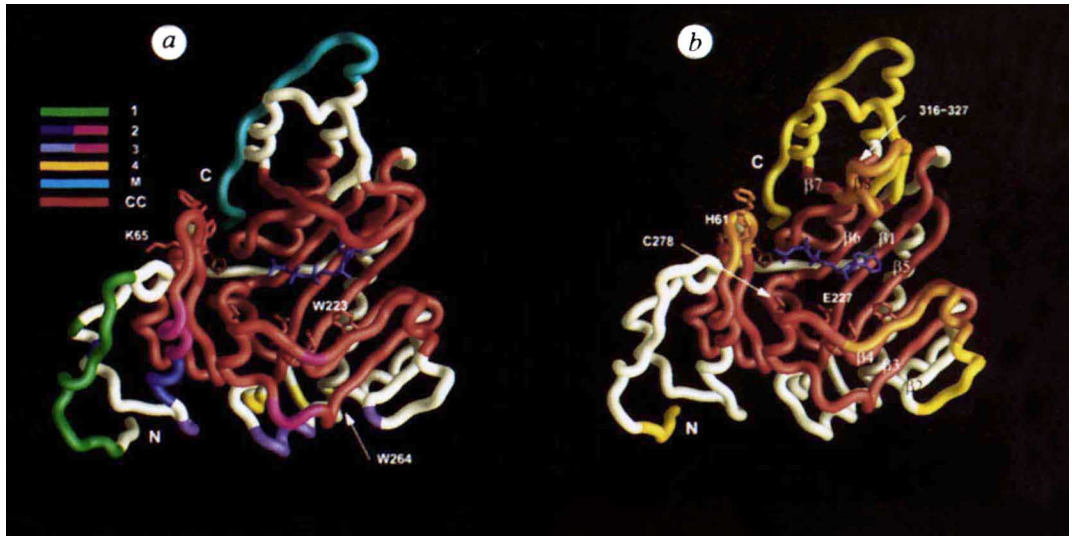

FIG. 1 Monomer structure. The course of the polypeptide chains is shown in the 'worm' representation, provided by the graphics program GRASP (A. Nicholls). The bound ATP is in blue. The common core (CC, red) of conserved amino-acid residues of CK isoenzymes includes the catalytic centre of the molecule. The conserved regions are Ile 52–His 92, Tyr 120–Ile 132, Gln 180–Lys 242, Phe 266–His 291, Arg 311–Val 325 and Asp 330–Val 352. Structural differences between the four crystallographically independent monomers in the octamer are rare, comprising residues 1–10, 60–66, 109–120, 313–327, and the position of the bound nucleotide. The structures of monomers A, C and D (*a*) are roughly the same but pronounced differences are found in monomer B (*b*). *a*, Assembly into octamers involves four contact regions in each monomer: contact 1 (green), Lys 5–Lys 20 and Pro 31; contact 2 (blue), Tyr 34 and Ser 47–Cys 51 (pink), Ile 52–Asn 58; contact 3 (violet), Asn 44–Gly 45, Ser 142–Arg 147 and Thr 172 (pink), Lys 191 and Arg 204–Trp 206; contact 4 (yellow), Gly 134–Ser 136, Glu 261–Trp 264. The pink regions in contacts 2 and 3 are also part of the conserved region. The region M (light blue), Lys 360–Lys 380, is involved in binding to the negatively charged head groups of lipids in the minochondrial membranes. *b*, Flexible segments of the polypeptide chain of monomer B with temperature factors above 40 Å^2 are yellow, or orange if they are also part of the conserved region. The locations of the flexible loops 60–65 and 314–331, and the strands β_1 to β_8, as defined in *c*, are indicated. *c*, Schematic representation of secondary structure. First and last amino-acid residues in the helices and sheet strands are specified according to the automatic procedure DSSP[30]. Each monomer can be partitioned into two domains: the small domain I consists of a 3_{10}-helix and five α-helices of which helix α_3 is distorted; the large domain II contains a central 8-stranded antiparallel β-sheet surrounded by seven α-helices. A second β-sheet of three very short antiparallel strands (Trp 268–Asn 269, Gly 273–Tyr 274, Gly 283) has been omitted. *d*, Stereo pair of a representative portion of the final $2F_o - F_c$ map covering residues Phe 189, Trp 206 and Trp 223. Density is contoured at 20% of the map maximum.

c

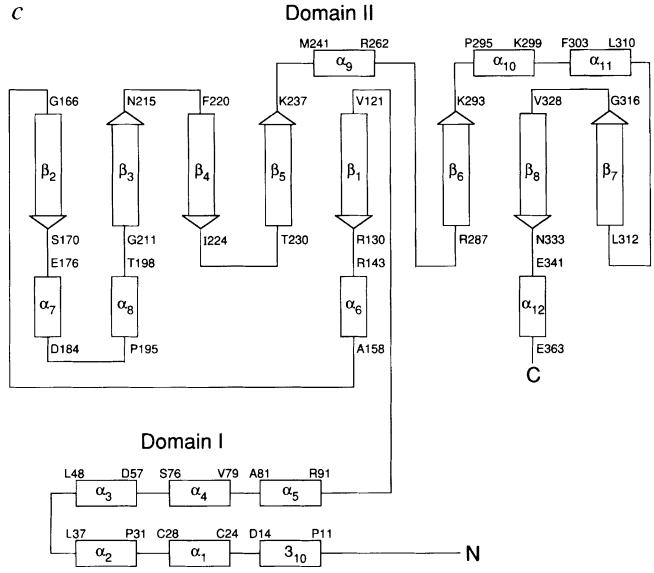

d

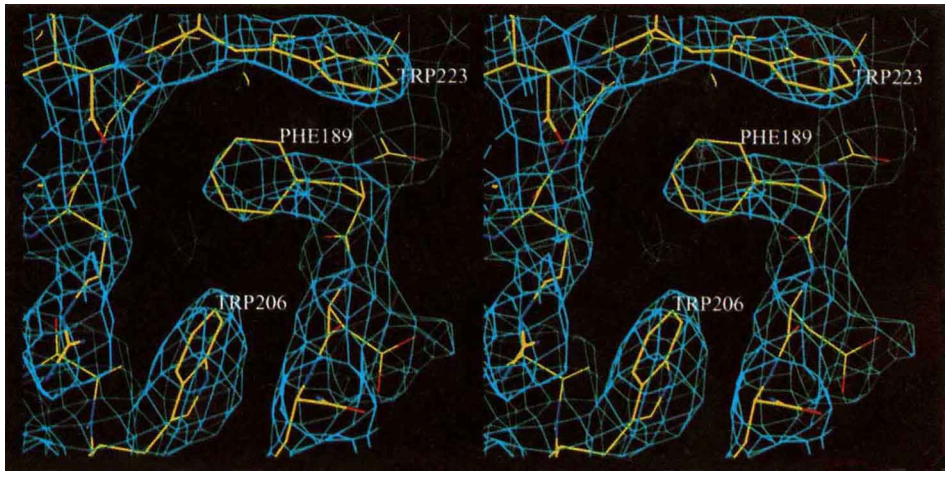

TABLE 1 Statistics of crystallographic data

Resolution bins (Å):	Overall	∞–6.0	6.0–5.0	5.0–4.0	4.0–3.5	3.5–3.0
ATP : Mi_b-CK		($a = b = 126.0$ Å, $c = 144.8$ Å)				
R_{sym} (%) (3 crystals)*	9.4	4.1	6.9	8.3	15.9	35.5
Mean redundancy†	3.3	3.7	3.9	3.7	3.2	2.7
Completeness (%)	96.7	93.7	99.3	98.7	98.0	95.4
of data with $I > \sigma$	72.3	89.1	90.8	86.7	76.0	52.0
R (%)‡	22.7	26.8	22.0	18.3	22.2	29.0
R_{free} (%)§	27.9	34.5	27.8	22.6	26.3	34.1
Mi_b-CK (native)		($a = b = 126.0$ Å, $c = 144.7$ Å)				
R_{sym} (%) (7 crystals)*	11.4	6.7	9.6	11.3	20.3	39.7
Mean redundancy†	6.0	9.8	7.9	7.4	6.1	3.3
Completeness (%)	99.5	99.1	100.0	100.0	100.0	99.0
of data with $I > \sigma$	88.0	98.5	98.4	97.7	93.6	73.3
R (%)‡	21.7	26.5	21.8	17.5	20.5	27.2
R_{free} (%)§	26.4	32.2	26.6	22.2	24.0	31.4
Mean figure of merit	0.47	0.51	0.41			
PCMB61		($a = b = 126.1$ Å, $c = 145.1$ Å)				
Completeness (%)	85.1	86.8	82.6			
Phasing power‖	1.6	1.8	1.3			
R_C (%)¶	53.4	48.3	69.7			
PCMB3		($a = b = 125.8$ Å, $c = 145.0$ Å)				
Completeness (%)	99.7	99.4	100.0			
Phasing power‖	1.6	1.9	1.2			
R_C (%)¶	50.4	46.4	62.9			

Sarcomeric Mi_b-CK was purified from chicken myocardium[16]. Enzymatic activity was verified by measuring the H^+ consumption in the reaction[18,24]. For crystallization, the protein solution was dialysed against buffer (in mM) (25 sodium phosphate, 1 NaN_3, 2 β-mercaptoethanol, 0.2 Na_2EDTA, pH 6.7) and diluted to 5 mg ml^{-1}. Crystals (space group $P4_2$, $a = 126.0$ Å, $c = 144.7$ Å) were grown at room temperature by the hanging-drop technique, using 17% PEG 1,000 (Merck) as precipitant in the above buffer. In the drop, the initial concentration of the protein was 2.5 mg ml^{-1}, while that of the precipitant was half the concentration in the reservoir solution. These crystals are better suited for X-ray analysis than the other forms described previously[25,26]. Co-crystals of the new type were grown in the presence of 5 mM NaATP (Boehringer) in the drop solution. After data collection, the co-crystals were freed from unbound ATP and analysed on a Superose 12 gel-permeation fast protein liquid chromatography column (Pharmacia) for verification that ATP was present in the crystals. X-ray diffraction images were collected at 4 °C by the rotation method and processed by the program XDS[27]. Native and heavy-atom derivative crystal data were recorded by an electronic area detector (Siemens/Nicolet, Madison, WI; crystal-to-detector distance, 13 cm; exposure time per image, 3–4 min; rotation range per image, 0.1–0.01°) using X-rays (CuK_α-line from a rotating anode operated at 35 kV and 50 mA, GX-18 Elliott/Enraf-Nonius, Delft) focused by Franks double-mirror optics. Two heavy-atom derivative data sets (PCMB3 and PCMB61) were obtained by soaking native crystals in mother liquor containing 22% PEG 1,000 and 2 mM *p*-chloromercuribenzoate (Sigma) for 6 and 12 h at room temperature. Diffraction data from the ATP : Mi_b-CK co-crystals were recorded by an imaging plate detector (X-rayresearch, Hamburg; crystal-to-detector distance, 25 cm; rotation range per image, 1°) using synchrotron radiation (wavelength, 0.91 Å) at the EMBL-outstation (DESY). Structure determination used programs from W.K. (unpublished), and X-PLOR[28] and O[29] for refinement and model building, respectively. Analysis of the native data set, Mi_b-CK (native), by the rotation function revealed 422 point-group symmetry of the Mi_b-CK octamer. One of the two-fold axes coincides with a crystallographic two-fold axis; the four-fold symmetry axis is in the *ab* plane of the crystal at an angle of 77.3° to the *a*-axis. The unit cell contains two octamers with the centres at the special positions 0, 1/2, 0 and 1/2, 0, 1/2, respectively. Deconvolution of the difference Patterson maps of the PCMB-derivatives revealed 4 (data set PCMB61) or 8 (data set PCMB3) heavy-atom sites related by the non-crystallographic symmetry of the octamer. Phase information to 3 Å resolution was extracted from the four-fold redundancy of the density in the asymmetric unit. The complete atomic model was obtained by several rounds of model building and correction followed by refinement and map calculation. The strict non-crystallographic symmetry was slightly relaxed in the final stages of refinement as the amino-acid chain adopts different conformations in each monomer for residues 1–10, 60–66, 109–120 and 313–327. The geometry of the atomic model, which contains no water molecules, is close to standard values with an average deviation of 0.007 Å in bond distances and 1.2° in bond angles. Apart from the peptide connecting Trp 206 with Pro 207, which is probably in a *cis*-conformation, the average deviation from the ideal *trans*-conformation is 7°. Uncertainties in the structure assignments remain for loop residues 316–326, 60–66 and the first five residues at the N terminus (located in weak electron density). The ATP : Mi_b-CK structure was solved using the native model.

* $R_{sym} = \sum_h \sum_i |I_{hi} - I_h| / \sum_{hi} I_{hi}$, where h are unique reflection indices and I_{hi} are the intensities of symmetry equivalent reflections giving a mean value of I_h.

† Multiplicity of measurements of each unique reflection.

‡ $R = \sum |F_{obs} - F_{model}| / \sum F_{obs}$, where F_{obs} and F_{model} are observed and atomic-model structure factor amplitudes, respectively. Reflections at resolution lower than 8 Å are excluded from the summation.

§ *R*-factor calculated for 10% of the reflections excluded from the refinement.

‖ Phasing power is the mean value of the heavy-atom structure factor amplitude divided by the residual lack-of-closure error.

¶ Cullis *R*-factor for centric reflections.

results of nuclear magnetic resonance (NMR) studies, from which a distance of 7–10 Å between the manganese ion of MnADP and the nitroxide moiety of the spin-label attached to Cys 278 was estimated[10].

A carboxyl group, which must be ionized for the binding of both creatine and phosphocreatine, has been implicated from studies of pH rate[11]. In the X-ray structure we find Asp 228, Glu 227 and Glu 226 (lower right in Fig. 2*a*) as possible candidates which, in addition, could be involved in coordinating the magnesium ion of ATP. The first two residues are also in the vicinity of Cys 278, which is thought to mark the creatine-binding site[9], as mentioned above. Asp 335, which has been radioactively labelled by ClRATP, an ATP analogue with the reactive label covalently bound to the γ-phosphate group[12], forms a salt bridge with Arg 311, and its side chain is pointing away from Cys 278 and the phosphate moiety of ATP (lower left in Fig. 2*a*), which makes it less likely that this residue is involved in creatine binding.

The presence of arginine and lysine residues in the catalytic site has been inferred from chemical modification and NMR studies (reviewed in refs 1,2). The X-ray structure reveals five arginines and one lysine in the catalytic region of the molecule. The side chain of Lys 314 is pointing away from the nucleotide, which suggests that it has a more indirect role during catalysis.

NMR studies on the role of histidines at the active site have revealed four such residues at distances 12, 12, 14 and > 18 Å from the Cr^{3+} in the paramagnetic β,γ-bidentate Cr^{3+} ATP complex bound to the enzyme[13]. One of these residues, with a pK near 7, was postulated to act as an acid–base catalyst[11]. We find His 92, His 291, His 229, His 61 and His 186 at distances of 12, 12,

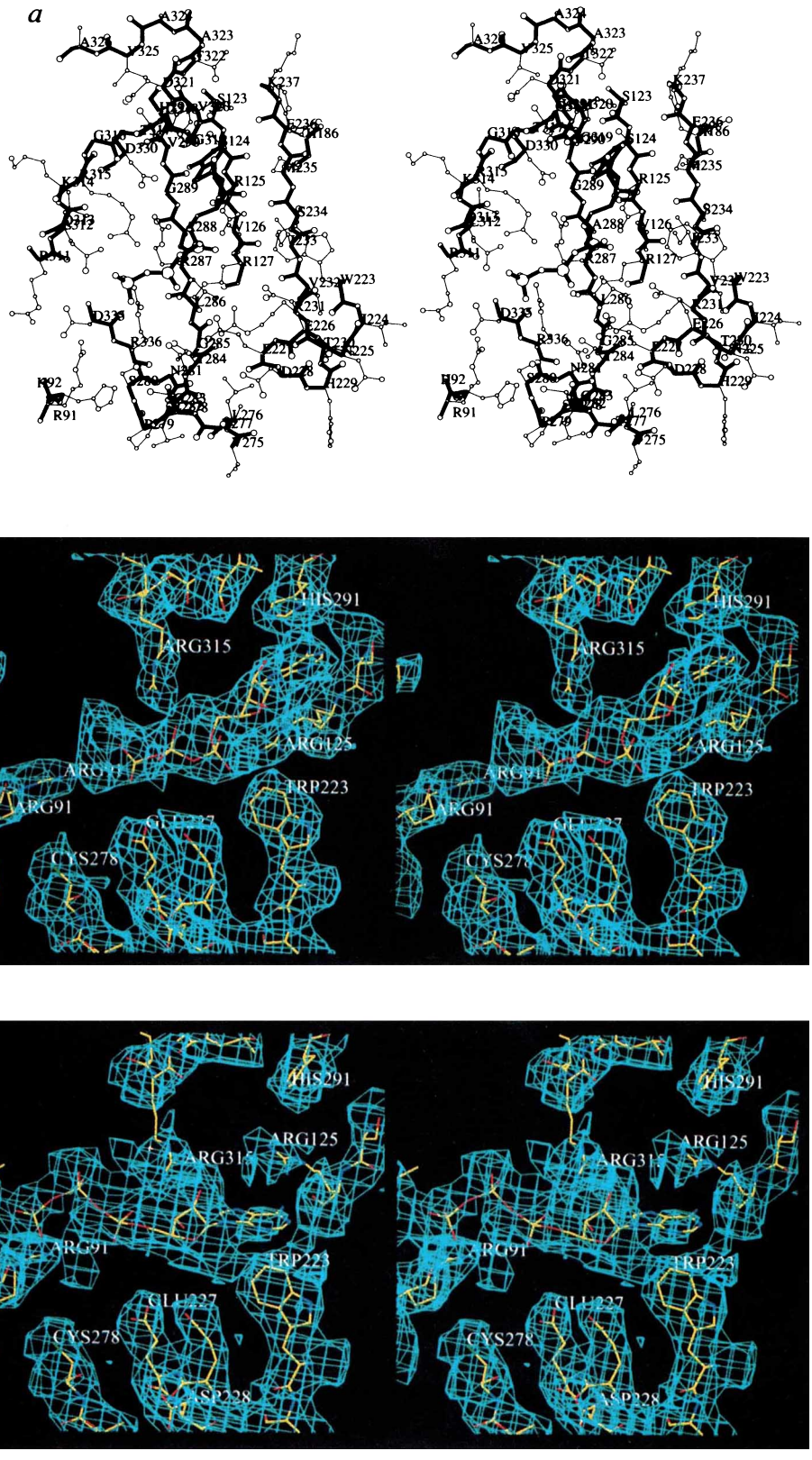

FIG. 2 Stereo pairs of the active site of Mi_b-CK. *a*, Atomic details of the nucleotide-binding region in monomer A (similar to monomers C and D). The adenine base fits into a pocket formed by residues Met 235, His 186, Ser 123, His 291, Gly 289, Arg 125 and the pair Arg 287, Asp 330, which forms a salt bridge. There are no specific interactions between these amino acids and the adenine base which is found in the anti orientation relative to the ribose. The dihedral angle χ of the *N*-glycosidic bond is $\sim -134°$. The phosphate groups of ATP interact with five arginine residues at positions 287, 125, 127, 315 and 336, with two (125 and 127) belonging to strand β_1, which connects the domains. An additional residue, Arg 91, is 5.4 Å from the γ-phosphate. *b*, Omit map of the nucleotide and some neighbouring residues in monomer A. Electron density was obtained using computed phases from the atomic model refined without ATP. Density is contoured at 10% of the map maximum. *c*, Omit map of the nucleotide in monomer B (same view and contour level as *b*). Consistent with the higher temperature factor, the density is less well defined than for the nucleotides in the other monomers.

14, 17 and 18 Å from the O7 atom of ATP, respectively (Fig. 2*a*). His 92 is closest to the γ-phosphate and to Cys 278. However, we cannot exclude that His 61, which resides on a flexible loop thought to be involved in the structural reorganization during catalysis, could also approach the active site. Thus we can only speculate that His 92 or possibly His 61 could function as the general acid–base catalyst.

The presence of a tryptophan residue in the vicinity of the adenine part of the substrate (< 5 Å) has been deduced from NMR and fluorescence-spectroscopic observations[14]. It was later shown by site-directed mutagenesis that replacement of Trp 223 results in a complete inactivation of the enzyme[15]. In the X-ray structure, Trp 223 is at a larger distance, about 10 Å, from the adenine (middle right in Fig. 2*a*,*b*) but, as mentioned above, we

expect that the nucleotide would approach Trp 223 in the presence of Mg^{2+}.

Mi_b-CK octamers are quite stable, the dissociation into dimers upon dilution taking hours to weeks[16,17]. This process is greatly accelerated by the addition of a transition-state analogue-complex mixture (TSAC = creatine, MgADP and nitrate)[18], which leads to dissociation within minutes[17]. The dimers of all CK isoforms are very stable, and disintegrate into monomers only under chaotropic conditions. The crystal structure explains the observed stability of the octamer and its assembly from dimers by numerous interactions of its monomers (Fig. 3). Most of the contacts involve isotype-specific regions in the amino-acid sequence outside the conserved CK framework[5]. Exceptions are Ile 52 to Asn 58 in contact region 2, and residues Lys 191 and Arg 204 to Trp 206 in contact region 3, which are also conserved residues (Fig. 1*a*). This is consistent with the finding that these residues are involved in the formation of CK dimers, which is a common property of both the mitochondrial and cytosolic isoforms of CK. Form and size of the dimers and their orientation in the octamer agree well with results of electron microscopy[19]. Moreover, the contribution of Trp 206 in contact region 3 to the stability of the dimers has been shown by site-directed mutagenesis and fluorescence spectroscopy[15].

Trp 264 has been suggested to be part of a hydrophobic inter-

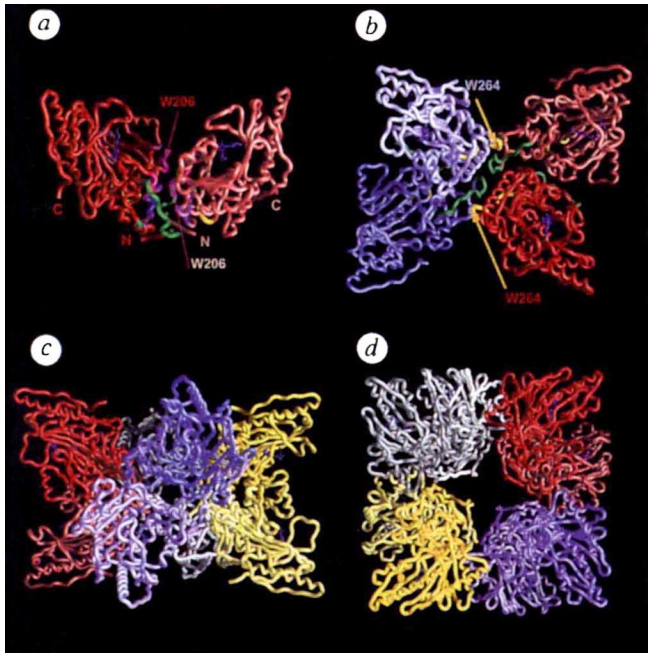

FIG. 3 Assembly of the Mi_b-CK octamer from monomers. The course of the polypeptide chains is shown in the 'worm' representation provided by the graphics program GRASP (A. Nicholls). The assembly involves four contact regions in each monomer, as defined in Fig. 1*a*. Regions 1–3 are used for dimer formation, and contacts 1 and 4 for the formation of octamers. The solvent-accessible areas[30] of a monomer, dimer and octamer are 17,057, 31,427 and 119,317 Å^2, respectively. Thus dimer formation reduces the sum of the accessible areas of its monomers by 2,687 Å^2, which is even larger than the contact area of 1,849 Å^2 in the tight complex between actin and DNase I. The accessible area of the octamer, assembled from four dimers, is reduced by 6,391 Å^2. The amino-acid residues involved in the interactions form a hydrophobic cluster which is shielded from solvent. *a*, Dimer formation. Two monomers, shown in red and light red, assemble into elongated dimers (length 92 Å, width 42 Å), which are shaped like bananas. The position of Trp 206 in contact region 3 is indicated. *b*, Assembly of two dimers. The position of Trp 264, a residue that is known to contribute to the stability of the octamer by contacting an N-terminal region 1 (green) of a neighbouring dimer, is indicated. *c*, Assembly of the Mi_b-CK octamer from four dimers. The viewing direction is roughly along a two-fold axis of the octamer. *d*, View of the Mi_b-CK octamer along its four-fold symmetry axis. A channel of diameter 20 Å extends through the whole octamer.

dimer-interaction patch important for octamer stability, because replacement of this residue by cysteine drastically increases the TSAC-induced dissociation and the sensitivity of the octamer to salt[15,17]. Moreover, the role of the amino-terminal heptapeptide (region 1) in stabilizing the hydrophobic interaction cluster has been confirmed by several mutants in this region, all of which resulted in a shift of the equilibrium from the octameric towards the dimeric form[20].

Side and top views of the Mi_b-CK octamer are shown in Fig. 3*c*, *d*. The complex fits into a tetragonal cell of dimensions 93 × 93 × 86 Å. A channel of diameter 20 Å extends along the four-fold axis through the octamer (Fig. 3*d*). The N termini of the monomers protrude into the channel at half height, whereas the C termini are located at the top and bottom four-fold faces. Dimensions and symmetry of the octamer are in excellent agreement with results from electron microscopy[19,21,22]. It has also been shown that the octamers preferentially bind with their four-fold faces to the negatively charged phospholipid head groups of inner and outer mitochondrial membranes, mainly by electrostatic interaction[21,23]. The C-terminal region Lys 360 to Lys 380 (M in Fig. 1*a*), located at the four-fold faces of the octamer, contains several positively charged amino acids. It is likely that some of the residues Lys 360, Lys 361, Lys 364, Lys 369, Arg 379 and Lys 380, and possibly also His 113 and Lys 110, are involved in the binding of Mi_b-CK octamers to naturally occurring cardiolipin of the mitochondrial inner membrane, and to the negatively charged head groups of lipids found in the outer membrane. The membrane-binding regions identified in the structure could explain the ability of Mi_b-CK to mediate the observed adhesion between inner and outer mitochondrial membranes[23], and make it plausible that Mi-CK, the only isoform in the CK system to form octamers, has evolved to serve this additional function as a structural protein. □

Received 13 November 1995; accepted 29 March 1996.

1. Watts, D. C. *The Enzymes* 3rd edn (ed. Boyer, P. D.) 383–455 (Academic, New York, 1973).
2. Kenyon, G. L. & Reed, G. H. *Adv. Enzymol.* **54,** 367–426 (1983).
3. Wallimann, T., Wyss, M., Brdiczka, D., Nicolay, K. & Eppenberger, H. M. *Biochem. J.* **281,** 21–40 (1992).
4. Hossle, J. P. *et al. Biochem. biophys. Res. Commun.* **151,** 408–416 (1988).
5. Mühlebach, S. M. *et al. Molec. cell. Biochem.* **133/134,** 245–263 (1994).
6. Taylor, S. S. & Radzio-Andzelm, E. *Structure* **2,** 345–355 (1994).
7. Wyss, M., James, P., Schlegel, J. & Wallimann, T. *Biochemistry* **32,** 10727–10735 (1993).
8. Olcott, M. C., Bradley, M. L. & Haley, B. E. *Biochemistry* **33,** 11935–11941 (1994).
9. Buechter, D. D., Medzihradszky, K. F., Burlingame, A. L. & Kenyon, G. L. *J. biol. Chem.* **267,** 2173–2178 (1992).
10. Taylor, J. S., Leigh, J. S. & Cohn, M. *Proc. natn. Acad. Sci. U.S.A.* **64,** 219–226 (1969).
11. Cook, P. F., Kenyon, G. L. & Cleland, W. W. *Biochemistry* **20,** 1204–1210 (1981).
12. James, P., Wyss, M., Lutsenko, S., Wallimann, T. & Carafoli, E. *FEBS Lett.* **273,** 139–143 (1990).
13. Rosevear, P. R., Desmeules, P., Kenyon, G. L. & Mildvan, A. S. *Biochemistry* **20,** 6155–6164 (1981).
14. Vašák, M., Nagayama, K., Wüthrich, K., Mertens, M. L. & Kägi, J. H. R. *Biochemistry* **18,** 5050–5055 (1979).
15. Gross, M., Furter-Graves, E. M., Wallimann, T., Eppenberger, H. M. & Furter, R. *Protein Sci.* **3,** 1058–1068 (1994).
16. Schlegel, J. *et al. J. biol. Chem.* **263,** 16942–16953 (1988).
17. Gross, M. & Wallimann, T. *Biochemistry* **34,** 6660–6667 (1995).
18. Milner-White, E. J. & Watts, D. C. *Biochem. J.* **122,** 727–740 (1971).
19. Schnyder, T., Engel, A., Lustig, A. & Wallimann, T. *J. biol. Chem.* **263,** 16954–16962 (1988).
20. Kaldis, P., Furter, R. & Wallimann, T. *Biochemistry* **33,** 952–959 (1994).
21. Schnyder, T., Cyrklaff, M., Fuchs, K. & Wallimann, T. *J. struct. Biol.* **112,** 136–147 (1994).
22. Schnyder, T., Gross, H., Winkler, H., Eppenberger, H. M. & Wallimann, T. *J. Cell Biol.* **112,** 95–101 (1991).
23. Rojo, M., Hovius, R., Demel, R. A., Nicolay, K. & Wallimann, T. *J. biol. Chem.* **266,** 20290–20295 (1991).
24. Wallimann, T., Schlösser, T. & Eppenberger, H. M. *J. biol. Chem.* **259,** 5238–5246 (1984).
25. Schnyder, T., Winkler, H., Gross, H., Eppenberger, H. M. & Wallimann, T. *J. biol. Chem.* **266,** 5318–5322 (1991).
26. Schnyder, T., Sargent, D. F., Richmond, T. J., Eppenberger, H. M. & Wallimann, T. *J. molec. Biol.* **216,** 809–812 (1990).
27. Kabsch, W. *J. appl. Crystallogr.* **26,** 795–800 (1993).
28. Brünger, A. T. *X-PLOR Version 3.1* (Yale University, New Haven, CT, 1992).
29. Jones, T. A., Zou, J. Y., Cowan, S. W. & Kjeldgaard, M. *Acta crystallogr.* A**47,** 110–119 (1991).
30. Kabsch, W. & Sander, C. *Biopolymers* **22,** 2577–2637 (1983).

ACKNOWLEDGEMENTS. We thank K. C. Holmes and H. M. Eppenberger for support; I. Schlichting for discussions and help collecting synchrotron data; D. Madden for reading the manuscript; G. Eulefeld, W. Gebhard and I. Naundorf for technical assistance with figures and system programming; D. Sargent for help during the initial phase of structure analysis; and members of the CK group, especially M. Forstner, R. Furter, E. Furter, M. Gross, W. Hemmer and M. Wyss for contributions. This work was supported by the ETH-Zürich, Swiss National Science Foundation, H. Horten Foundation, Swiss Muscle Foundation, and Careal Holding AG.

CORRESPONDENCE and requests for materials should be addressed to W.K. (e-mail: kabsch@mpimf-heidelberg.mpg.de). The coordinates have been deposited in the Brookhaven Protein Databank, accession number 1crk, where they will be held for one year before release.